Letter

High-Efficiency Orientation Insensitive WPT Systems Using Magnetic Dipole Coil for Low-Power Devices

Cancan Rong, Xiangrui He, Yingqin Zeng, Conghui Lu, and Minghai Liu

***Abstract*—In this letter, a novel kind of coupling mechanism for orientation insensitive and superior transmission performance is proposed. The transmitting coil is comprised of a cubic-type magnetic dipole, which can achieve relatively omnidirectional wireless charging. The receiving coil has two dipole coils that are perpendicular to each other, guaranteeing a maximum magnetic flux reception from the transmitter. The proposed coupling mechanism is verified by the ANSYS Maxwell software. *LCC*-S compensation topology is implemented to achieve load-independent and constant-voltage output simultaneously. The reasonable size of the prototype is fabricated, and the experimental results show that the stable efficiency and output power can be achieved against rotational misalignment. Our new coil structure designs significantly improve the free degree of direction and may provide a flexible power supply to low-power devices.**

***Index Terms*—Crossed-type receiver, cubic-shaped transmitter, *LCC*-S compensation topology, magnetic dipole, wireless power transfer (WPT) system.**

I. Introduction

WIRELESS power transfer (WPT) technology has been recognized as an eye-catching research hotspot and developing rapidly in the world. By virtue of its remarkable advantages of convenience, reliability, and low maintenance, WPT technology has been used in various industrial applications, such as the electrical vehicles, portable electronic equipment, and implantable medical devices [1]–[3]. At present, most WPT works focus on planar resonance coils, which carry out directional power flow and are seriously affected by the misalignment and orientation [4]–[6]. Along with the increasing development of WPT technology as well as expanding application requirements, particularly, the studies on the orientation insensitive draw a great deal of attention and interest from researchers around the world [7]–[13].

Manuscript received November 2, 2021; revised December 7, 2021; accepted December 16, 2021. Date of publication December 21, 2021; date of current version January 19, 2022. *(Corresponding author: Xiangrui He.)*

Cancan Rong is with the School of Electrical and Power Engineering, China University of Mining and Technology, Xuzhou 221116, China (e-mail: ccrong@cumt.edu.cn).

Xiangrui He, Yingqin Zeng, Conghui Lu, and Minghai Liu are with the School of Electrical and Electronic Engineering, Huazhong University of Science and Technology, Wuhan 430074, China (e-mail: xiangruihe@hust.edu.cn; yqzeng@hust.edu.cn; conghuilu@hust.edu.cn; mhliu@hust.edu.cn).

Color versions of one or more figures in this article are available at https://doi.org/10.1109/TPEL.2021.3137225.

Digital Object Identifier 10.1109/TPEL.2021.3137225

Among them, Ng *et al.* [7] proposed three orthogonal coils and a nonidentical current control method for omnidirectional WPT systems. In [8], a bowl-shaped coil with multiple transmitters was designed to generate a homogenous magnetic field for charging a planar receiver with an arbitrary position. In [9], a quadrature-shaped receiver was applied to achieve an angular-misalignment insensitive WPT systems. In [10], a trifoliate coil in the form of a three-phase transformer was investigated, which can realize great system efficiency tolerance for misalignment. In [11], a cubic transmitter was proposed to achieve the omnidirectional WPT systems with relatively high efficiency at 13.56 MHz. In [12], three crossed-loop square transmitters were used, and current amplitude/phase angle control was also used to ensure three-dimensional magnetic field orientation. In [13], the crossed coils with an orthogonal phased difference for the transmitter have been adopted for generating *DQ* rotating magnetic field. In summary, the specific construction design of the resonator (especially transmitter) and current modulation are two basic considerations for orientation insensitive WPT systems in these state-of-the-art studies. However, the multiple-phase current regulation will increase the complexity of the circuitry and the cost of the system. Besides, the control method will add unnecessary burden on the systems, such as communication and module feedback control.

A good compensation network can significantly enhance the controllability of orientation insensitive WPT systems, which can greatly simplify the system redundancy [14]. Unfortunately, the research articles into compensation topology for omnidirectional WPT systems are insufficient. The majority of primary works tended to adopt S–S compensation network because of its simple structure and relatively great property (the resonant frequency is irrelevant to the coupling coefficient and load resistor). However, other compensation topologies, such as *LCC* and *LCL* topology, can present exciting performances on certain occasions [15]. In [16], *LCC–LCC* topology was used to ensure current flowing stable under rotation condition. In [17], *LCL*-P topology was adopted for continuous and discontinuous current. The disadvantage of this topology is low tolerance against misalignment. In [18], three-phase *LCC*-S topology was chosen to keep the power constant for multiple loads.

In order to realize steady output power and transmission efficiency under rotational condition, this letter proposes the cubic transmitter and corresponding cross-type receiver based

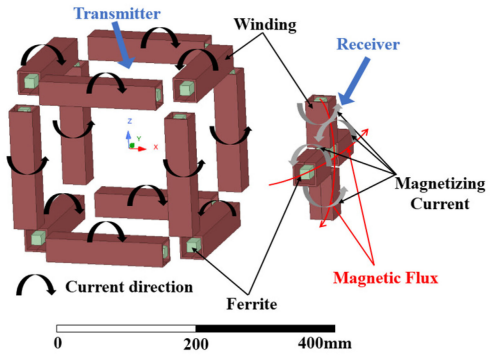

Fig. 1. General overview of the proposed omidirecitonal coil structrue.

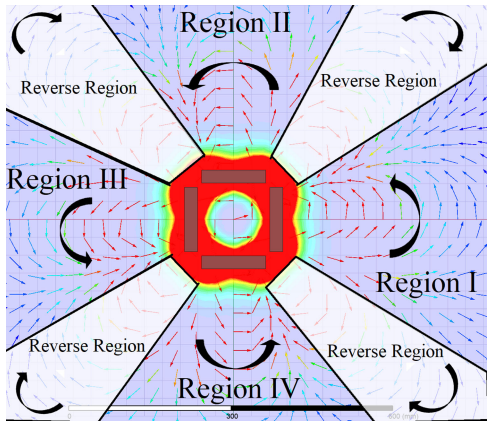

Fig. 2. Magnetic field vector diagram in the *XOY*-plane generated by the cubic transmitter.

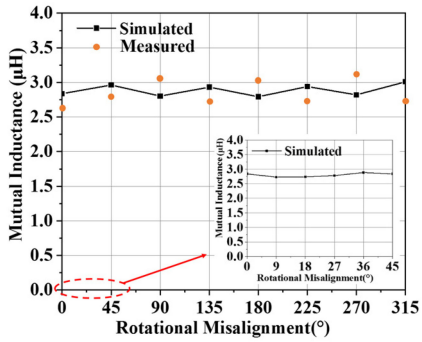

Fig. 3. Simulated and measured mutual inductances.

on a magnetic dipole coil to ensure enough magnetic coupling. The proposed coil structure is validated via ANSYS Maxwell software. *LCC*-S component topology is adopted to ensure the constant-current and constant-voltage output. The current control module is not required for overall systems. An orientation insensitive wireless charging prototype is set up to verify the studies.

II. Magnetic Structure Design

The general overview of the proposed magnetic structure is shown in Fig. 1. It is worth mentioning that the diagram is just used to display the magnetic structure; the multiturn windings wrapped in the ferrite are replaced by a cuboid-shaped coil for better demonstration and simulation analysis. It has been proved that the ferrite coil can generate much stronger electromagnetic field than the air coil due to lower magnetic reluctance [19]. Cubic-shaped transmitter consists of 12 magnetic dipoles connected in series and there are 2^{12} combinations of the current direction theoretically. In order to enhance the magnetic couplings between the cubic transmitter and the crossed receiver, the current direction of each dipole is set to produce a uniform magnetic field around the transmitter. For the maximum induction of the magnetic flux from the transmitter, a cross-type receiver consists of four dipoles, which are linked in series as well. The magnetic flux directions through the receiver are perpendicular to each other. The ingenious design ensures a relatively constant and strong magnetic coupling between the dipole coils.

Honestly, the cubic-shape transmitter and crossed-type receiver have been proposed already in the previous articles, as stated before. However, the greatest innovation of this letter is the special winding methods of the transmitter and receiver and the adaptive interaction of both resonant coils based on magnetic dipole coil to achieve maximum magnetic coupling. Fig. 2 depicts the magnetic field vector diagram in the *XOY*-plane generated by the cubic transmitter. It can be seen that the direction of the magnetic field is anticlockwise in all of the transmitting regions I, II, III, and IV. Note that the reverse region certainly exists to satisfy the closed magnetic field line. Meanwhile, the direction of the vertical magnetic field can be determined easily because the four vertical dipole coils of the cubic transmitter share the same current directions. Based on the above demonstrations, the winding directions of the four dipole coils of the receiver can be determined because the phase of the horizontal and vertical induced voltage can be settled by the fixed magnetic field directions.

In order to verify the omnidirectional characteristic of the proposed magnetic structure, the mutual inductances between the transmitter and receiver changing with the rotational misalignments are simulated and measured. The comparison results are shown in Fig. 3, where the operating frequency is set to 85 kHz. It can be seen that the mutual inductance remains relatively constant versus rotational misalignments and the measured results agree well with the simulated ones. Four cases of different winding methods are given for comprehensive comparison in the Appendix; it can be found that the mutual inductances between the transmitter and receiver changing with the rotational misalignments vary largely.

III. Compensation Network Analysis

The circuit topology (*LCC*-S compensation network) for the proposed WPT systems is shown in Fig. 4. L_P and L_S are the inductances of the primary and secondary winding, respectively. The primary series compensation is performed by connecting the compensation capacitor C_P in series with the transmitting coil. Together with the tuning series inductor L_R and parallel capacitor C_R, these three components form the *LCC* primary resonant circuit. The secondary winding compensation is implemented by

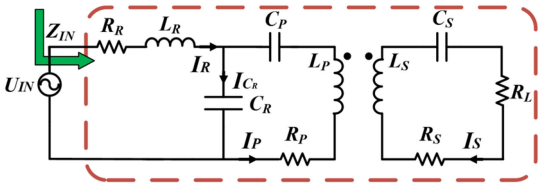

Fig. 4. Proposed *LCC*-S compensation topology.

common series capacitor C_S. R_R, R_P, and R_S are the parasitic resistors of the L_R, L_P, and L_S, respectively. An equivalent series resistor R_L denotes both the secondary switching controller and the load resistance. $Z_{\rm IN}$ represents the input impedance from the *LCC*-S topology.

To achieve the constant-current output of the primary winding and constant-voltage output on the load of the secondary side, at the same time to meet the maximum efficiency, the operating frequency and various electric parameters need to satisfy [14]

$$\begin{cases} j\omega L_R + 1/j\omega C_R = 0 \\ j\omega L_P + 1/j\omega C_P + 1/j\omega C_R = 0 \\ j\omega L_S + 1/j\omega C_S = 0. \end{cases} \tag{1}$$

At resonance, the input impedance $Z_{\rm IN}$ of *LCC*-S compensation network can be calculated as

$$Z_{\rm IN} = R_R + \frac{p^2\omega^2 L_P^2}{(R_P + Z_f)} \approx \frac{p^2\omega^2 L_P^2}{(R_P + Z_f)} \tag{2}$$

where

$$\begin{cases} p = L_R/L_P \\ Z_f = (\omega M)^2 \Big/ R_L. \end{cases} \tag{3}$$

Since the parasitic resistances of these windings are relatively small compared with the impedances of compensation components, these parameters can be ignored due to limited effects on the resonant characteristic. In addition, it can be seen that the inductor factor p satisfies $0<p<1$ based on (1), which means L_R is smaller than L_P.

The current in each branch of the *LCC*-S topology can be calculated as (4). It is worth mentioning that the phase of $\dot{U}_{\rm IN}$ is taken as a reference

$$\begin{cases} \dot{I}_R = \frac{\dot{U}_{\rm IN}}{Z_{\rm IN}} = \frac{R_P + Z_f}{p^2\omega^2 L_P^2} U_{\rm IN} \angle 0^\circ \\ \dot{I}_P = \dot{U}_{\rm IN} G_c = \frac{U_{\rm IN}}{p\omega L_P} \angle -90^\circ \\ \dot{I}_{C_R} = \dot{I}_P - \dot{I}_R \\ \dot{I}_S = \frac{\dot{U}_{\rm out}}{Z_S} = \frac{G_v \dot{U}_{\rm IN}}{R_L + R_S} = \frac{M U_{\rm IN}}{p L_P (R_L + R_S)} \angle 0^\circ \end{cases} \tag{4}$$

where the term $G_c = I_p/U_{\rm IN} = 1/\omega L_R$ is the current gain, and the term $G_v = U_{\rm out}/U_{\rm IN} = M/L_R$ is the voltage gain. $U_{\rm out}$ is defined as the voltage of the load resistor.

Hence, the real power $P_{\rm out}$ and the power transfer efficiency (PTE) can be written as follows:

$$\begin{cases} P_{\rm out} = I_S^2 R_L = \frac{M^2 R_L U_{\rm IN}^2}{p^2 L_P^2 (R_S + R_L)^2} \\ {\rm PTE} = \frac{P_{\rm out}}{U_{\rm IN} I_R} = \frac{\omega^2 M^2 R_L}{R_P (R_S + R_L)^2 + \omega^2 M^2 (R_S + R_L)}. \end{cases} \tag{5}$$

According to (5), PTE is independent of the inductor factor p, whereas closely related to the load resistor R_L. To reach the maximum PTE, the optimal load $R_{L\_\rm optimal}$ can be calculated by making the first derivative of PTE

$$R_{L\_\rm optimal} = R_L|_{\frac{\partial \eta}{\partial R_L}=0} = \sqrt{R_S^2 + \frac{R_S}{R_P}\omega^2 M^2} \approx \omega M. \tag{6}$$

It is of great significance that the *LCC*-S compensation network meets the resonant requirements, which can maximize PTE effectively. Here, another term q is introduced to study the fundamental PTE characteristics for a general *LCC*-S topology. It should be noted that the secondary coil is well matched to the optimal load. q is defined as follows:

$$q = (1/\omega C_P)/\omega L_P. \tag{7}$$

How PTE varies with p and q is analyzed by parametric sweeping. Fig. 5 shows the sweeping results for an exemplary case. It can be found from Fig. 5(a) that PTE reaches the maximum when the sum of p and q is equal to 1 from the contour lines, which is in consistent with (1) above. In addition, it can be seen from Fig. 5(b) that PTE is not that sensitive and remains relatively high when the p or q is larger than 1. Overall results provide useful guidelines for the parameter design of *LCC*-S topology.

Fig. 6 shows the magnitude and phase of the input impedance as a function of the operating frequency at different loads and coupling coefficients. It can be seen that frequency splitting for

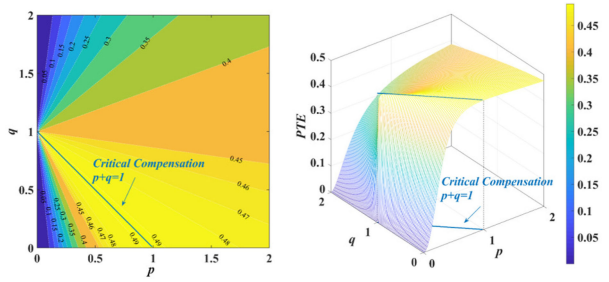

Fig. 5. Senstivity of PTE varies with p and q. (a) Contour of PTE. (b) Surface figure.

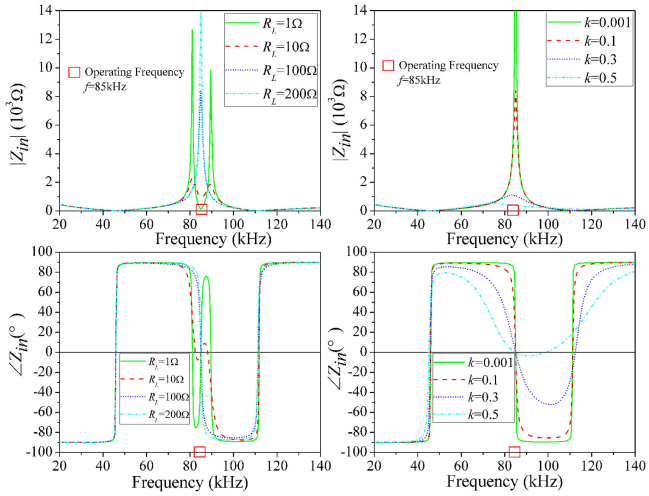

Fig. 6. Frequency-domain response. Magnitude of impedance varying with (a) load resistor and (b) coupling coefficient. Phase of the impedance varying with (c) load resistor and (d) coupling coefficient.

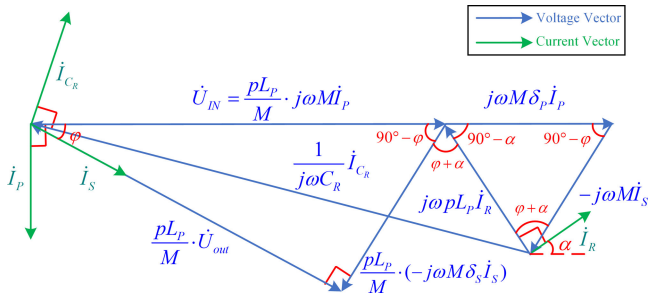

Fig. 7. Vector diagram of current/voltage under mistuned condition.

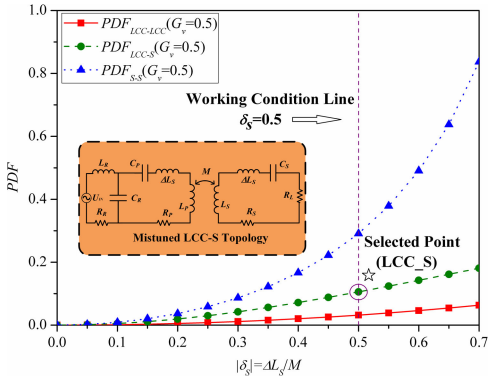

Fig. 8. Comparison diagram of PDFs vary with δ_S for S–S, *LCC–LCC*, and proposed *LCC*-S compensation topologies.

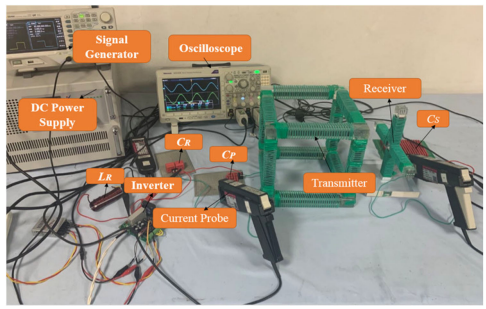

Fig. 9. Prototype of the proposed WPT system.

impedance magnitude occurs when the load is small, as shown in Fig. 6(a). However, this bifurcation phenomenon does not happen when the coupling coefficients vary, and the impedance magnitude is more stable when the magnetic coupling is stronger. Therefore, the results indicate that the bifurcation is mainly caused by the reflected impedance of the receiver. Meanwhile, high reactive power is injected into the network when bifurcation occurs, indicating a drop of PTE. Detailed mistuning analysis is shown as follows. The phase curves of impedance intersect the zero-phase line at multiple points (up to five points), as shown in Fig. 6(c) and (d). It means that the input impedance is not pure resistance only in the case of magnetically coupling resonance at 85 kHz. However, compared with other zero points, this magnetic resonance state is the most stable because it is not affected by the load and coupling coefficient.

The usage of a ferrite core can enhance the magnetic coupling between the transmitter and receiver. However, demagnetization will occur when the magnetizing field is generated in the ferrite core, resulting in core losses that cannot be ignored during the analysis. The effect for demagnetization can be described by the variation of the inductance, causing the mistuned for the compensation topology circuit. The basic characteristics of the mistuned S–S and *LCC–LCC* compensation topology have been analyzed in [20] in detail. Therefore, only the mistuned properties of *LCC*-S topology are discussed in this letter.

The mistuned terms $\delta_p = \Delta L_p/M$ and $\delta_s = \Delta L_s/M$ are defined to illustrate the primary and secondary variations of the inductances, assuming that φ is the phase of $\dot{U}_{\text{out}}$ and α is the phase of $\dot{I}_R$. Hence, according to the KVL, the vector diagram for the voltage and current can be drawn as Fig. 7, where blue vectors represent the voltage and green means the current. Hence, voltage gain under mistuned condition G_{v_mistuned} can be expressed as

$$G_{v\_\text{mistuned}} = \frac{U_{\text{out}}}{U_{\text{in}}} = \frac{M}{pL_P}\cdot\frac{1}{\sqrt{1+\delta_S^2}} = G_v\cdot\frac{1}{\sqrt{1+\delta_S^2}} \tag{8}$$

where δ_p gets eliminated in the simplification process. For the specific coupling mechanism proposed by this letter, since δ_S is almost determined when the current flow in the secondary side circuit is ensured, G_{v_mistuned} is only related to p.

The mistuned output power $P_{\text{out\_mistuned}}$ is derived as

$$P_{\text{out\_mistuned}} = \frac{1}{\omega pL_P\delta_S}U_{\text{IN}}U_{\text{out}}\left|\sin\varphi\right|. \tag{9}$$

The output power displacement factor (PDF) is defined in [20], where the PDF for *LCC*-S topology can be obtained as (10), which varies with the secondary side δ_S

$$\text{PDF} = \left|\frac{P_{\text{out\_mistuned}} - P_{\text{out}}}{P_{\text{out}}}\right| = \sqrt{\frac{1}{1+\delta_S^2}} - 1. \tag{10}$$

Considering the power level for the wireless network sensor, we set $G_{v\_\text{mistuned}} = 0.5$. Based on the article presented in [20], the PDFs vary with δs for S–S, and *LCC–LCC* compensation topologies are compared with *LCC*-S topology proposed in this letter, as shown in Fig. 8. The PDF of S–S topology is larger than that of *LCC*-S topology, while *LCC–LCC* is less than *LCC*-S. It means that the power displacement of *LCC–LCC* topology is minimal when the inductance is detuned. However, *LCC–LCC* topology needs more components than *LCC*-S topology, causing difficulties to tune and design the systems. In addition, U_{out} is related to the load R_L for *LCC–LCC* topology due to its *V–C* property [14], while *LCC*-S network realizes the constant-voltage output. From all the demonstrations above, the *LCC*-S compensation topology is preferred in this letter. When $G_{v\_\text{mistuned}} = 0.5$, p can be calculated by (8), which equals 0.0055.

IV. Experimental Verification

An experimental prototype based on the magnetic dipole coil is constructed, as shown in Fig. 9. The proposed WPT system specifications and circuit parameters are tabulated in Table I. The experimental results of various parameters are well matched to

TABLE I
CIRCUIT PARAMETERS OF THE PROPOSED WPT SYSTEMS

Parameters	Value	Parameter	Value	Parameter	Value
f_0	85kHz	L_R	5.40μH	C_R	650.0nF
U_{IN}	10V	L_P	980.17μH	C_P	3.6nF
R_L	1.6Ω	L_S	253.12μH	C_S	14.0nF

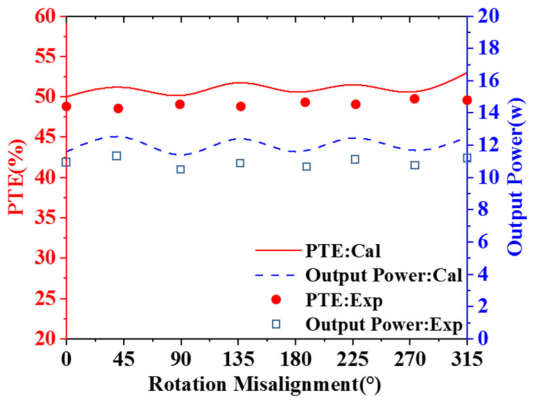

Fig. 10. PTE and output power against rotational misalignments.

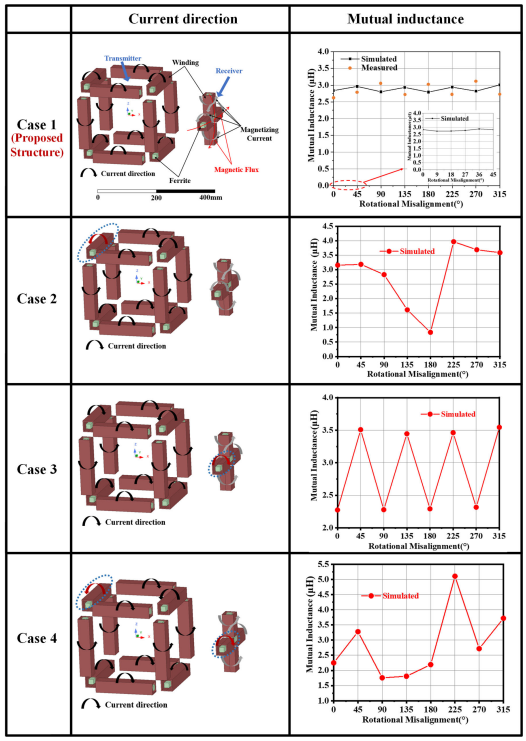

Fig. 11. Mutual inductances of different current directions of resonators for four arbitrary cases.

the simulations. Fig. 10 depicts the system transfer efficiency and output power against the rotational misalignments. The measured results agree well with the calculated ones. PTE and output power remain relatively constant versus rotational misalignments. Under the condition that the transmission distance is about twice the length of the magnetic dipole, the efficiency can achieve about 50% and deliver above 10 W output power.

V. CONCLUSION

The orientation insensitive WPT systems based on magnetic dipole coil have been proposed. *LCC*-S compensation topology is analyzed in detail, especially for special properties of ferrite under mistuned condition and other typical compensation networks compared. It can reach about 50% stable efficiency in the case of rotation at a relatively long distance. These designs can be applicable to low-power scenarios (about 10 W), such as wireless sensors and moving robot.

APPENDIX

Four cases of different winding methods for the cubic-shaped transmitter and cross-type receiver and corresponding mutual inductances between the transmitter and receiver changing with the rotational misalignments are given in Fig. 11. They are as follows:

1) the proposed structure in the letter;
2) the current direction of one of the transmitter changes (mark with red color);
3) the current direction of one of the receiver changes (mark with red color);
4) the current direction of one of the transmitters and one of the receivers changes (mark with red color).

REFERENCES

[1] Z. Li, C. Zhu, J. Jiang, K. Song, and G. Wei, "A 3-kW wireless power transfer system for sightseeing car supercapacitor charge," *IEEE Trans. Power Electron.*, vol. 32, no. 5, pp. 3301–3316, May 2017.
[2] S. Jeong *et al.*, "Smartwatch strap wireless power transfer system with flexible PCB coil and shielding material," *IEEE Trans. Ind. Electron.*, vol. 66, no. 5, pp. 4054–4064, May 2019.
[3] Y. Palagani, K. Mohanarangam, J. H. Shim, and J. R. Choi, "Wireless power transfer analysis of circular and spherical coils under misalignment conditions for biomedical implants," *Biosensors Bioelectron.*, vol. 141, Sep. 2019, Art. no. 111283.
[4] S. Wang, Z. Hu, C. Rong, C. Lu, J. Chen, and M. Liu, "Planar multiple-antiparallel square transmitter for position-insensitive wireless power transfer," *IEEE Antennas Wireless Propag. Lett.*, vol. 17, no. 2, pp. 188–192, Feb. 2018.
[5] S. Y. Hui, "Planar wireless charging technology for portable electronic products and Qi," *Proc. IEEE*, vol. 101, no. 6, pp. 1290–1301, Jun. 2013.
[6] J. P. K. Sampath, A. Alphones, and D. M. Vilathgamuwa, "Figure of merit for the optimization of wireless power transfer system against misalignment tolerance," *IEEE Trans. Power Electron.*, vol. 32, no. 6, pp. 4359–4369, Jun. 2017.
[7] W. M. Ng, C. Zhang, D. Lin, and S. Y. Ron Hui, "Two- and three-dimensional omnidirectional wireless power transfer," *IEEE Trans. Power Electron.*, vol. 29, no. 9, pp. 4470–4474, Sep. 2014.
[8] J. Feng, Q. Li, F. C. Lee, and M. Fu, "Transmitter coils design for free-positioning omnidirectional wireless power transfer system," *IEEE Trans. Ind. Informat.*, vol. 15, no. 8, pp. 4656–4664, Aug. 2019.
[9] Z. Zhang and B. Zhang, "Angular-misalignment insensitive omnidirectional wireless power transfer," *IEEE Trans. Ind. Electron.*, vol. 67, no. 4, pp. 2755–2764, Apr. 2020.
[10] H. Matsumoto, Y. Neba, H. Iura, D. Tsutsumi, K. Ishizaka, and R. Itoh, "Trifoliate three-phase contactless power transformer in case of winding-alignment," *IEEE Trans. Ind. Electron.*, vol. 61, no. 1, pp. 53–62, Jan. 2014.
[11] N. Ha-Van and C. Seo, "Analytical and experimental investigations of omnidirectional wireless power transfer using a cubic transmitter," *IEEE Trans. Ind. Electron.*, vol. 65, no. 2, pp. 1358–1366, Feb. 2018.

[12] Q. Zhu, M. Su, Y. Sun, W. Tang, and A. P. Hu, "Field orientation based on current amplitude and phase angle control for wireless power transfer," *IEEE Trans. Ind. Electron.*, vol. 65, no. 6, pp. 4758–4770, Jun. 2018.

[13] B. H. Choi, E. S. Lee, Y. H. Sohn, G. C. Jang, and C. T. Rim, "Six degrees of freedom mobile inductive power transfer by crossed dipole Tx and Rx coils," *IEEE Trans. Power Electron.*, vol. 31, no. 4, pp. 3252–3272, Apr. 2016.

[14] W. Zhang and C. C. Mi, "Compensation topologies of high-power wireless power transfer systems," *IEEE Trans. Veh. Technol.*, vol. 65, no. 6, pp. 4768–4778, Jun. 2016.

[15] C. Jiang, K. T. Chau, C. Liu, and C. H. T. Lee, "An overview of resonant circuits for wireless power transfer," *Energies*, vol. 10, no. 7, Jun. 2017, Art. no. 894.

[16] Z. Yan, B. Song, Y. Zhang, K. Zhang, Z. Mao, and Y. Hu, "A rotation-free wireless power transfer system with stable output power and efficiency for autonomous underwater vehicles," *IEEE Trans. Power Electron.*, vol. 34, no. 5, pp. 4005–4008, May 2019.

[17] C.-S. Wang, G. A. Covic, and O. H. Stielau, "Investigating an *LCL* load resonant inverter for inductive power transfer applications," *IEEE Trans. Power Electron.*, vol. 19, no. 4, pp. 995–1002, Jul. 2004.

[18] L. Tan *et al.*, "Power stability optimization design of three-dimensional wireless power transmission system in multi-load application scenarios," *IEEE Access*, vol. 8, pp. 91843–91854, 2020.

[19] C. Park, S. Lee, G.-H. Cho, and C. T. Rim, "Innovative 5-m-off-distance inductive power transfer systems with optimally shaped dipole coils," *IEEE Trans. Power Electron.*, vol. 30, no. 2, pp. 817–827, Feb. 2015.

[20] W. Li, H. Zhao, J. Deng, S. Li, and C. C. Mi, "Comparison study on SS and double-sided *LCC* compensation topologies for EV/PHEV wireless chargers," *IEEE Trans. Veh. Technol.*, vol. 65, no. 6, pp. 4429–4439, Jun. 2016.